

SceneDreamer360: Text-Driven 3D-Consistent Scene Generation with Panoramic Gaussian Splatting

Wenrui Li¹, Yapeng Mi¹, Fucheng Cai¹, Zhe Yang², Wangmeng Zuo¹,
Xingtao Wang¹, Xiaopeng Fan¹

¹Harbin Institute of Technology

²University of Electronic Science and Technology of China

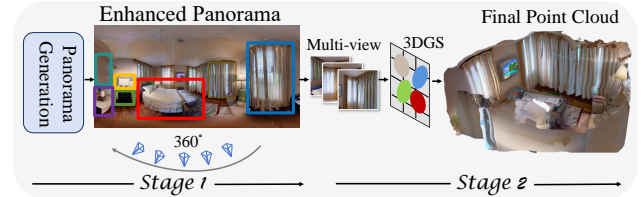
liwr@stu.hit.edu.cn, 2021111124@stu.hit.edu.cn, 2021113246@stu.hit.edu.cn, 202221110110@std.uestc.edu.cn
wmzuo@hit.edu.cn, xtwang@hit.edu.cn, fxp@hit.edu.cn

Abstract

Text-driven 3D scene generation has seen significant advancements recently. However, most existing methods generate single-view images using generative models and then stitch them together in 3D space. This independent generation for each view often results in spatial inconsistency and implausibility in the 3D scenes. To address this challenge, we proposed a novel text-driven 3D-consistent scene generation model: SceneDreamer360. Our proposed method leverages a text-driven panoramic image generation model as a prior for 3D scene generation and employs 3D Gaussian Splatting (3DGS) to ensure consistency across multi-view panoramic images. Specifically, SceneDreamer360 enhances the fine-tuned Panfusion generator with a three-stage panoramic enhancement, enabling the generation of high-resolution, detail-rich panoramic images. During the 3D scene construction, a novel point cloud fusion initialization method is used, producing higher quality and spatially consistent point clouds. Our extensive experiments demonstrate that compared to other methods, SceneDreamer360 with its panoramic image generation and 3DGS can produce higher quality, spatially consistent, and visually appealing 3D scenes from any text prompt. Our codes are available at <https://github.com/liwrui/SceneDreamer360>.

Introduction

The scarcity of annotated 3D text-point cloud datasets presents significant challenges in training 3D point cloud models directly from user queries, especially for complex 3D scenes. This challenge arises primarily because the cost-intensive nature of acquiring and annotating 3D data, coupled with the high precision required for modeling intricate 3D scenes. Consequently, existing methods often extend high-quality 2D generative models by leveraging 2D object priors to transition into 3D neural radiance fields. For instance, CLIP-NeRF (Wang et al. 2022) employs the CLIP (Radford et al. 2021) model to control the shape and appearance of 3D objects via textual prompts or images. Dream Fields (Jain et al. 2022) integrates neural rendering with image and text representations to generate diverse 3D objects from natural language descriptions. Similarly, Dreamfusion (Poole et al. 2022a) optimizes NeRF without requiring 3D training data, relying solely on a pre-trained 2D text-to-image diffusion model for text-to-3D synthesis.



“A bedroom with a double bed, bedside tables with lamps, a dresser with a mirror, and a large window with sheer curtains.”

Figure 1: We introduce SceneDreamer360, a text-based 3D scene generation framework designed to create realistic 3D scenes with high consistency across different viewpoints.

Despite significant advancements in NeRF-based point cloud generation methods, generating consistent point clouds with fine-grained details remains a challenge. The Text2Room (Höller et al. 2023) method often generates point clouds that are discontinuous, lack fine details, and require extended rendering times. Similarly, LucidDreamer (Chung et al. 2023) generates panoramic point clouds with numerous inconsistencies, resulting in incomplete panoramas. PanFusion (Zhang et al. 2024) also faces difficulties in generating panoramic images from complex long texts, leading to blurred areas and object deformations. Additionally, PanFusion’s panoramic images have a relatively low resolution (512×1024), leading to fewer spatial points corresponding to pixel points, which causes the rendered point clouds to appear blurred and fall short of ideal quality. To address these challenges, we propose introducing 3D Gaussian Splatting (3DGS) (Kerbl et al. 2023) for multi-scene generation, with a focus on producing more finely detailed complex scene point clouds. 3DGS utilizes Gaussian distribution for scene modeling, enabling finer representation of complex scene point clouds and enhancing reconstruction accuracy. Furthermore, with an optimized rendering algorithm, 3DGS significantly reduces rendering times while maintaining high quality, resulting in more efficient generation outcomes.

In this paper, we propose a novel SceneDreamer360 for text-driven 3D-consistent scene generation using panoramic Gaussian splatting. As shown in Fig. 1, our approach uses a two-stage process: panoramic image enhancement for 3D

consistency priors, followed by 3DGS to reconstruct high-quality, text-aligned point clouds. For panorama generation and enhancement, existing methods enhance image resolution through iterative progressive scene rendering, often leading to consistency issues between successive renderings. To address this, we fine-tune the PanFusion (Zhang et al. 2024) model by incorporating an MLP (Murtagh 1991) and LoRA (Hu et al. 2021) layer at the final stage, training it using the Habitat Matterport Dataset (Ramakrishnan et al. 2021). This approach yields a model checkpoint tailored to specific needs, enhancing the quality of panoramic image generation. We further enrich and upscale the panoramas using CN (Zhang, Rao, and Agrawala 2023) and RealESR-GAN (Wang et al. 2021), achieving resolutions up to 6K. This enhancement improves point cloud rendering, preserving high-resolution details for more aesthetically pleasing and realistic results. During point cloud fusion, we design a novel point cloud initialization method to enhance consistency and reduce rendering time. Additionally, leveraging the effective representation of 3DGS enables the generation of complete and detailed point cloud images. Our contributions can be summarised as follows:

- We propose SceneDreamer360, a domain-free high-quality 3D scene generation method, achieving better domain generalization in 3D scene generation by leveraging the panorama generation and 3D Gaussian Splatting.
- Our method adapts panorama generation to provide a consistency prior for scenes, fine-tunes the model, and applies a three-stage enhancement to add more detail and spatial consistency to the final scene generation.
- To improve scene reconstruction, we employed 3D Gaussian Splatting and introduced a novel point cloud initialization and fusion algorithm, resulting in enhanced performance of the final generated point cloud scenes.

Related Work

3D Scene Generation. The field of 3D scene generation has evolved significantly, drawing inspiration from various breakthroughs in image generation techniques. Early approaches leveraged Generative Adversarial Networks (GANs) (Goodfellow et al. 2014), attempting to create multi-view consistent images (Chan et al. 2021; Niemeyer and Geiger 2021) or directly generate 3D representations like voxels (Nguyen-Phuoc et al. 2019, 2020) and point clouds (Achlioptas et al. 2018; Shu, Park, and Kwon 2019). Later, the advent of diffusion models (Ho, Jain, and Abbeel 2020; Song, Meng, and Ermon 2020) and their success in image generation (Ramesh et al. 2021; Rombach et al. 2022) sparked a new wave of research in 3D scene generation. Researchers began applying diffusion models to various 3D representations, including voxels (Zhou, Du, and Wu 2021), point clouds (Vahdat et al. 2022), and implicit neural networks (Poole et al. 2022b). While these approaches showed promise, they often focused on simple, object-centric examples due to their inherent nature.

To address more complex scenarios, some generative diffusion models employed meshes as proxies, diffusing in UV space. This approach enabled the creation of large portrait

scenes through continuous mesh building (Fridman et al. 2024) and the generation of indoor scenes (Cohen-Bar et al. 2023; Lei, Tang, and Jia 2023) and more realistic objects (Qian et al. 2023). Currently, an increasing number of studies (Chung et al. 2023; Zhou et al. 2024b; Ma, Zhan, and Jin 2024; Li et al. 2024) have incorporated 3DGS (Kerbl et al. 2023) as a 3D representation to complement diffusion models in generating more complex 3D scenes. However, due to diffusion models generating one viewpoint at a time before merging and elevating to 3D space, the resulting 3D scenes often lack realism and consistency.

In contrast, to address the issues of quality and spatial consistency, our method leverages the promising 3D Gaussian Splatting technique and implements a three-stage enhancement process for the generated panoramic images. Concurrent work HoloDreamer (Zhou et al. 2024a) has explored similar concepts. However, our approach is distinguished by an innovative design in the panoramic image enhancement stage and a novel point cloud fusion algorithm.

3D Scene Representation. The field of 3D scene representation has evolved significantly, encompassing a variety of approaches with distinct trade-offs and applications. Traditional explicit methods such as point clouds, meshes, and voxels have long been fundamental to 3D modeling, offering intuitive control and fast rendering through rasterization. However, these methods often require a large number of elements to achieve high resolution, which can be computationally expensive. To address this limitation, more complex primitives are developed, including cuboids (Tulsiani et al. 2017) and polynomial surfaces (Yavartanoo et al. 2021), offering more efficient expression of geometry but still struggling with realistic color representation.

Recent advancements have led to the emergence of implicit neural representations, such as Signed Distance Functions (SDF) (Takikawa et al. 2021) and Neural Radiance Fields (NeRF) (Mildenhall et al. 2021). Among these advancements, 3D Gaussian Splatting (3DGS) (Kerbl et al. 2023) has emerged as a particularly promising approach. It represents complete and unbounded 3D scenes by effectively 'splatting' Gaussians, utilizing spherical harmonics and opacity for strong representational capabilities. 3DGS balances quality and efficiency by supporting alpha-blending and differentiable rasterization, enabling fast 3D scene optimization. It refines point clouds details through a split-and-clone mechanism, making it ideal for complex scene generation where scene bounds are uncertain.

Panorama Generation Panoramas offer a comprehensive, unobstructed view that captures extensive scene areas. Recent advancements in panorama generation have significantly improved the quality and consistency of 360-degree images. While early attempts like PanoGen (Li and Bansal 2024) and MultiDiffusion (Bar-Tal et al. 2023) used pre-trained diffusion models to create long images from text prompts, these methods often resulted in inconsistencies and lacked true panoramic properties. To address these limitations, researchers have developed more sophisticated approaches. MVDiffusion (Tang et al. 2023) introduced a correspondence-aware attention mechanism to generate consistent multi-view images simultaneously. StitchDiffusion

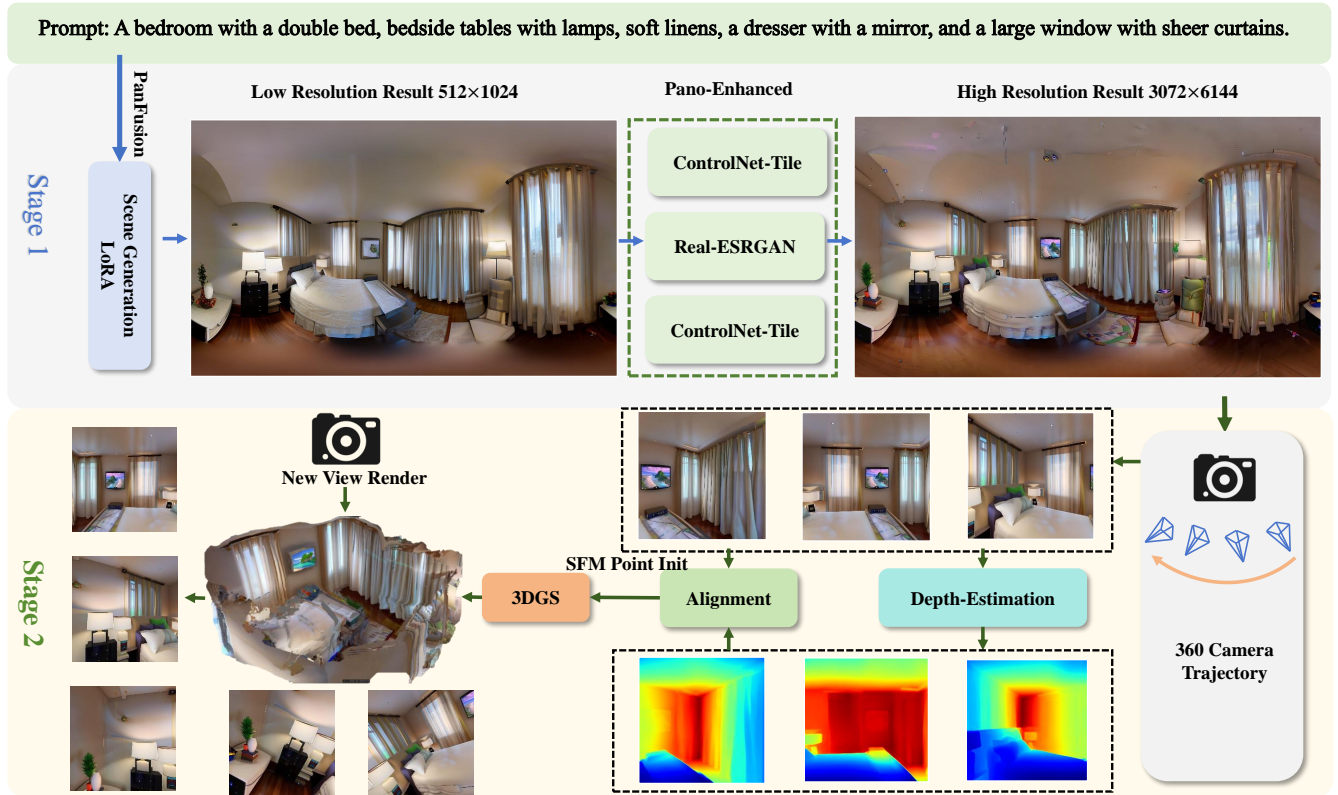


Figure 2: The architecture of the SceneDreamer360. SceneDreamer360 generates an initial panorama from any open-world textual description using the fine-tuned PanFusion model. This panorama is then enhanced to produce a high-resolution 3072×6144 image. In the second stage, multi-view algorithms generate multi-view images, and a monocular depth estimation model provides depth maps for initial point cloud fusion. Finally, 3D Gaussian Splatting is used to reconstruct and render the point cloud, resulting in a complete and consistent 3D scene.

(Wang et al. 2024) improved upon it by using LoRA (Hu et al. 2021) fine-tuning to generate complete 360-degree panoramas with enhanced continuity between image edges. PanFusion (Zhang et al. 2024) proposed a novel dual-branch diffusion model to generate a 360-degree image from a text prompt. In this paper, we incorporated MLP and LoRA into the PanFusion model and performed fine-tuning to enhance the consistency of the generated panoramic images.

Method

This method introduces a novel pipeline for generating high-resolution 360-degree panoramic point cloud scenes from arbitrary spatial text, consisting of two main stages: Panoramic Image Generation and Processing, and Point Cloud Construction with Gaussian Splatting. The overall pipeline of SceneDreamer360 is shown in Fig. 2 .

Panoramic Image Generation and Processing

The goal of Panoramic Image Generation and Optimization is to convert a long-text description of a complex scene into high-quality 360-degree panoramas with high resolution. The specific steps are as follows:

Panoramic Image Generation. Our method utilized the PanFusion model (Zhang et al. 2024) to generate panoramas. However, because the PanFusion model was originally trained on simple short text prompts, it required appropriate adjustments and fine-tuning to handle complex long texts. Therefore, we added a Multi-Layer Perceptron (MLP) (Murtagh 1991) layer and a Low-Rank Adaptation (LoRA) (Hu et al. 2021) layer to the original PanFusion model, fine-tuning it using the reannotated Habitat Matterport Dataset (Ramakrishnan et al. 2021). The MLP layer captures higher-order features in complex long texts, while the LoRA layer enhances the model’s representation ability through low-rank matrix decomposition. For model fine-tuning, we first reannotated the dataset using the generated complex long texts, pairing them with corresponding panoramas to form new training samples. Next, we froze the pre-trained parts of the PanFusion model and trained only the newly added MLP and LoRA layers. This ensures that the model effectively utilizes information from complex long texts to generate high-quality panoramas. These panoramas encapsulate the details and scenes described in the input text, serving as foundational data for subsequent steps.

Panoramic Image Optimization. As the pre-trained Pan-

Fusion model can only generate panoramas with a resolution of 512×1024 , directly using these panoramas for multi-view extraction and point cloud reconstruction would result in sparse point clouds with blurry 3D Gaussian rendering (Kerbl et al. 2023). To meet the requirements of point cloud reconstruction, it is necessary to further enhance the resolution and quality of the panoramas. The specific steps are as follows: We adopted a three-step super-resolution reconstruction method involving ControlNet-Tile (Zhang, Rao, and Agrawala 2023), RealESRGAN (Wang et al. 2021), and a second application of ControlNet-Tile to maximize the enhancement of image details and resolution.

Step 1: ControlNet-Tile Super-Resolution Reconstruction The ControlNet-Tile model divides the panorama into distinct tiles through semantic recognition. Each tile is analyzed by the model to determine which details to add and which parts to repair. Based on tiling, ControlNet-Tile enhances the details of each tile. The model can identify various areas in the image and enhance the details of each area, adding additional detail where necessary. The detail enhancement process can be expressed as:

$$\mathbf{I}_{enhanced} = f_{tile}(\mathbf{I}_{ori}, t), \quad (1)$$

where f_{tile} represents the ControlNet-Tile model, \mathbf{I}_{ori} represents the original panorama, and t represents the input text.

Step 2: RealESRGAN Super-Resolution Reconstruction Based on ControlNet-Tile, we further employed RealESRGAN for higher precision super-resolution reconstruction. RealESRGAN is an advanced super-resolution method based on generative adversarial networks, capable of enhancing resolution while preserving natural details and visual consistency. The super-resolution reconstruction process can be expressed as:

$$\mathbf{I}_{super} = g_{ESRGAN}(\mathbf{I}_{enhanced}), \quad (2)$$

where g_{ESRGAN} represents the RealESRGAN model.

Step 3: ControlNet-Tile Re-Optimization After RealESRGAN processing, we applied ControlNet-Tile once more for additional refinement and optimization. The purpose of this second application of ControlNet-Tile is to further enhance the details and quality of the image at the increased resolution. The final optimized image \mathbf{I}_{final} is represented as:

$$\mathbf{I}_{final} = f_{tile}(\mathbf{I}_{super}, t). \quad (3)$$

By following these steps, we increased the panorama’s resolution to 3072×6144 . This high-resolution panorama preserves the original image’s overall structure while significantly enhancing details and clarity, thus providing high-quality input data for subsequent point cloud reconstruction.

Multi-View Image Acquisition. After obtaining the high-resolution panorama, we need to extract images from specific viewpoints for point cloud reconstruction. We select a suitable set of camera poses $P_i \in \mathbb{R}^{4 \times 4}$ based on the requirements of point cloud reconstruction. The selection of these camera poses is based on geometric and visual coverage principles, ensuring that the chosen perspectives comprehensively cover important details and areas of the panorama. Specifically, we use an optimization-based viewpoint selection algorithm that considers the distribution of

viewpoints, parallax effects, and coverage of reconstruction areas. The camera pose P_i is represented as:

$$\mathbf{P}_i = \begin{bmatrix} \mathbf{R}_i & \mathbf{T}_i \\ \mathbf{0} & 1 \end{bmatrix}. \quad (4)$$

The rotation matrix R_i is expressed as:

$$\mathbf{R}_i = \begin{bmatrix} \cos(\theta) & 0 & \sin(\theta) \\ 0 & 1 & 0 \\ -\sin(\theta) & 0 & \cos(\theta) \end{bmatrix}. \quad (5)$$

The translation matrix T_i is expressed as:

$$\mathbf{T}_i = \begin{bmatrix} T_x \\ T_y \\ T_z \end{bmatrix} = \begin{bmatrix} 0 \\ 0 \\ 0 \end{bmatrix}. \quad (6)$$

By using the Equirectangular to Perspective (e2p) algorithm, we transformed the panorama to generate perspective images from specific viewpoints. The e2p algorithm converts spherical panoramas into multiple planar images from different viewpoints, thereby creating parallax between views. The perspective transformation formula is:

$$\mathbf{I}_{perspective}(\mathbf{u}, \mathbf{v}) = \mathbf{E}(\mathbf{P}(f(\mathbf{u}, \mathbf{v}), \mathbf{R}_i, \mathbf{T}_i), \mathbf{S}), \quad (7)$$

where $f(\mathbf{u}, \mathbf{v})$ represents the mapping function from planar coordinates (\mathbf{u}, \mathbf{v}) to spherical coordinates, \mathbf{S} represents the specified output size, \mathbf{E} and represents the view size transformation function.

By applying the above methods, we can generate high-quality 360-degree panoramas from input text prompts, providing high-resolution and detailed input data for subsequent point cloud reconstruction. Through precise perspective transformations, we obtained a set of viewpoint images that satisfy the requirements of point cloud reconstruction. These viewpoint images serve as a solid foundation for the subsequent point cloud reconstruction process.

Point Cloud Construction with Gaussian Splatting

After obtaining high-quality multi-view panoramic images, we apply the 3D Gaussian Splatting method for point cloud generation. We directly use 3D Gaussians to represent point clouds and have designed a novel point cloud alignment method. Additionally, we improved the point cloud initialization by applying masking to remove duplicates, resulting in a more refined and complete initial point cloud map. The point cloud reconstruction process is divided into two phases: Point Cloud Initialization and Rendering.

Point Cloud Initialization. The initial point cloud must be generated from multi-view images to enable reconstruction using 3D Gaussian Splatting (Kerbl et al. 2023). To generate a 360-degree spatial point cloud from multi-view images, a rendering trajectory centered around the observation viewpoint is required. This trajectory should cover the bottom, middle, and top of the spatial area. Using the Lucid-Dreamer (Chung et al. 2023) framework, we incorporate additional camera viewpoints to create a more accurate spatial point cloud. For the set of multi-view images $\mathbf{I}_1, \mathbf{I}_2, \dots, \mathbf{I}_n$ derived from the panoramic image, each image \mathbf{I}_i has a corresponding position \mathbf{P}_i . Using the monocular depth estimation model ZoeDepth (Bhat et al. 2023), we measure

the depth map \mathbf{D}_i for each \mathbf{I}_i , forming the depth map set $\mathbf{D}_1, \mathbf{D}_2, \dots, \mathbf{D}_n$. We initialize the point cloud using a cyclic generation approach. The camera’s intrinsic matrix and the extrinsic matrix of \mathbf{I}_0 are denoted as \mathbf{K} and \mathbf{P}_0 , respectively. The initial point cloud for a single viewpoint is derived using the following formula:

$$\rho_0 = \tau_{2 \rightarrow 3}(\mathbf{I}_0, \mathbf{D}_0, \mathbf{K}, \mathbf{P}_0), \quad (8)$$

where $\tau_{2 \rightarrow 3}(\cdot)$ is a function that elevates a 2D image to a 3D point cloud. This function generates an initial point cloud ρ_i , corresponding to a viewpoint P_i .

For point cloud fusion from different perspectives, we employed a masking method to remove duplicates. Specifically, we defined a mask \mathbf{M}_i for each generated ρ_i , where the mask projects the already generated ρ_{i-1} onto the 2D image space through the corresponding view \mathbf{P}_i . The projected part of the mask has values greater than 0, while the rest remains black with a value of 0. At the final stage of generation, we remove the duplicated parts that have already been projected, effectively merging the point clouds from different perspectives and reducing duplicate points. Meanwhile, we estimate the optimal depth scaling factor d_i to minimize the distance between the 3D points of the new image and the corresponding points in the original point cloud \mathbf{P}_{i-1} . Then, by multiplying the factor d_i with the measured depth map \mathbf{D}_i , we calculate the corrected depth map $d_i \mathbf{D}_i$, which is subsequently used for the generation of ρ_i . The complete process is illustrated in the following formula:

$$d_i = \operatorname{argmin}_d \left(\sum \|\tau_{2 \rightarrow 3}([\mathbf{I}_i, d\mathbf{D}_i], \mathbf{K}, \mathbf{P}_i) - \rho_{i-1}\|_1 \right), \quad (9)$$

$$\rho_i = \tau_{2 \rightarrow 3}(\mathbf{I}_i - \mathbf{M}_i, d_i \mathbf{D}_i, \mathbf{K}, \mathbf{P}_i), i \neq 0. \quad (10)$$

Finally, through continuous iteration of the formula, we fuse the point clouds to form the final point cloud Ω .

$$\Omega = \bigcup_{i=1}^{|P|} \varphi \{ \rho_i, \rho_{i-1} \}. \quad (11)$$

The function φ represents the depth alignment function, and all ρ are integrated to obtain the complete initial point cloud Ω . **The overall algorithm is shown in Algorithm 1.**

Rendering with Gaussian Splatting. 3D Gaussian Splatting is a technique that can quickly and efficiently model 3D scenes. After generating the point cloud, we use it to train a 3D Gaussian Splatting model. The generated point cloud Ω serves as the initial Structure from Motion (SfM) points. Initializing with Ω accelerates network convergence and encourages the network to focus on generating detailed representations. We utilize multi-view image slices as training images. Additionally, we apply the image view augmentation technique from LucidDreamer. Since the input multi-view images may not cover the complete 3D space, we project the Ω point cloud into 2D space from different camera viewpoints to increase the number of supervisory images. The formal representation are as follows:

$$\mathbf{I}_i, \mathbf{M}_i = \psi_{3 \rightarrow 2}(\Omega, \mathbf{K}, \mathbf{P}_i), \quad (12)$$

where $\psi_{3 \rightarrow 2}(\cdot)$ is the function that projects the 3D point cloud onto the 2D plane. Through this method, we achieve a more consistent and complete scene point cloud.

Algorithm 1: Point cloud initialization algorithm

Input: Panoramic multiview RGBD images $[\mathbf{I}_i, \mathbf{D}_i]_{i=0}^N$

Input: Camera intrinsic \mathbf{K} , extrinsics $\{\mathbf{P}_i\}_{i=0}^N$

Output: Complete point cloud Ω

```

1:  $\rho_0 = \tau_{2 \rightarrow 3}(\mathbf{I}_0, \mathbf{D}_0, \mathbf{K}, \mathbf{P}_0)$ 
2: for  $i = 1$  to  $N$  do
3:    $d_i = 1$ 
4:    $\mathbf{M}_i = \psi_{3 \rightarrow 2}(\rho_{i-1}, \mathbf{K}, \mathbf{P}_i)$ 
5:   while not converged do
6:      $\tilde{\rho}_i = \tau_{2 \rightarrow 3}(\mathbf{I}_i, d_i \mathbf{D}_i, \mathbf{K}, \mathbf{P}_i)$ 
7:      $\mathcal{L}_d \leftarrow \frac{1}{\|\mathbf{M}_i\|} \sum_{\mathbf{M}_i=1} \|\tilde{\rho}_i - \rho_{i-1}\|_1$ 
8:     Calculate  $\nabla_d \mathcal{L}_d$ 
9:      $d_i \leftarrow d_i - \alpha \nabla_d \mathcal{L}_d$ 
10:  end while
11:   $\rho_i = \tau_{2 \rightarrow 3}(\mathbf{I}_i - \mathbf{M}_i, d_i \mathbf{D}_i, \mathbf{K}, \mathbf{P}_i)$ 
12:   $\Omega = \rho_{i-1} \cup \rho_i$ 
13: end for
14: return  $\Omega$ 

```

Experiment

In this section, we conducted a thorough and comprehensive evaluation of our method to validate its superiority. We performed both qualitative and quantitative evaluations that our method can generate clearer and higher quality 3D scenes.

Implementation Details. Our method is implemented using PyTorch. In the first stage, we generate panoramic images using a modified PanFusion model. We fine-tune this model on the Habitat Matterport Dataset, incorporating MLP and LoRA layers to produce realistic 3D panoramic images. A three-step super-resolution reconstruction process, including ControlNet-Tile and RealESRGAN, enhances the resolution of these images to 3072×6144 . In the second stage, we adapt and modify the point cloud reconstruction component from LucidDreamer. For evaluation, we use GPT-4 to generate a set of prompts that cover a wide range of scene types. We assess the quality of our outputs using metrics such as CLIP-Score, PSNR, and others. Our experiments are conducted on an NVIDIA A100-80G GPU.

Baselines. We compare our SceneDreamer360 with the following baselines.

- TextToRoom (Höllerin et al. 2023) employs a mesh-based 3D representation, directly extracting meshes from inpainted RGBD images to represent watertight indoor environments.
- LucidDreamer (Chung et al. 2023) projects outpainted RGBD images onto a point cloud and then supervises the optimization of 3DGS by projecting multiple images from this point cloud. However, since LucidDreamer cannot directly generate 3D scenes from prompts, we utilize a diffusion model to generate condition images, allowing LucidDreamer to create scenes from text input.

Evaluation Metrics. Since there are no established evaluation metrics for 3D scene point clouds, we assess our method using metrics from prior work. We calculate the CLIP-Score (Hessel et al. 2021) to measure text-image consistency, employ CLIP-IQA (Wang, Chan, and Loy 2023)

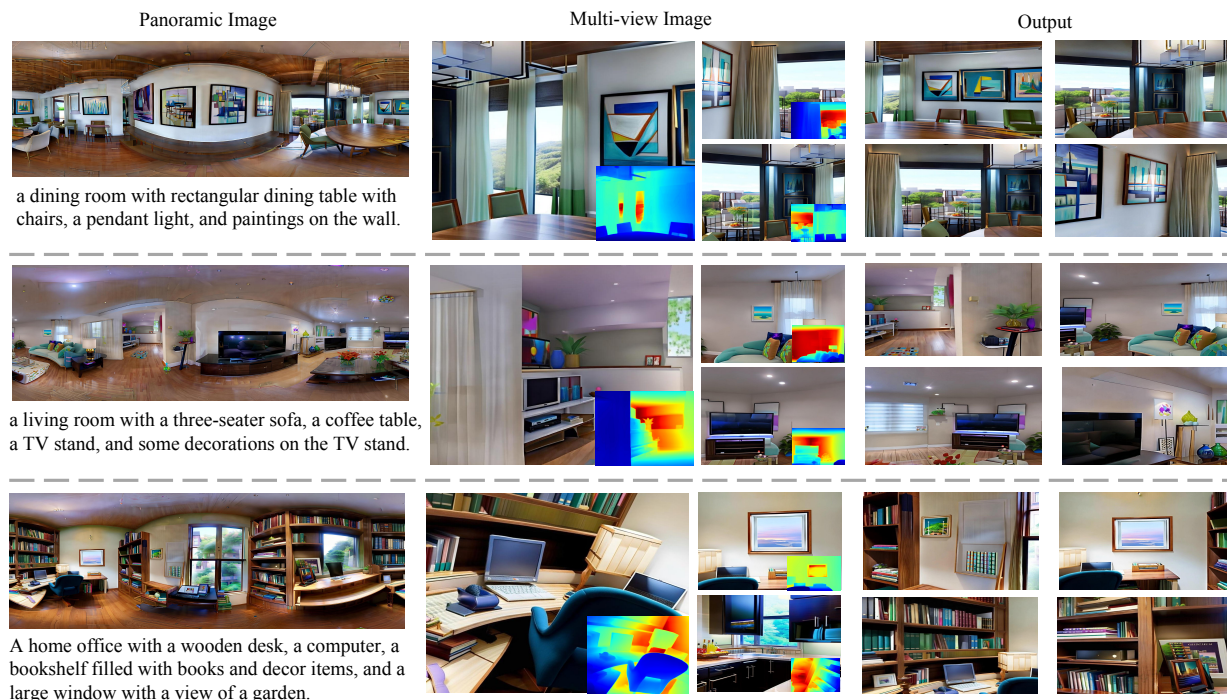


Figure 3: The visualization of SceneDreamer360. The Panoramic Image on the left represents the high-resolution enhanced panorama generated from a specific text input. The Multi-view Image shows different perspective images derived from the panorama, while the Output on the right displays images rendered from the generated point cloud at new viewpoints. As shown in the figure, SceneDreamer360 is capable of producing high-quality, detailed, and spatially consistent 3D scenes.

to evaluate image quality from a single viewpoint, and use PSNR, SSIM, and LPIPS to assess the quality of the rendered images.

Qualitative Result

The point cloud images generated by our method using different prompts are shown in Fig. 3. The method successfully generates 3D spatial scenes consistent with the text prompts. Additionally, part of the output demonstrates that images can be rendered from arbitrary trajectory views, showcasing the generalizability of our method. We visually compared our method with LucidDreamer and Text2Room using identical spatial text prompts, as shown in Fig. 4. Our method outperforms the others by producing more consistent, complete, and detailed 3D spatial scene point clouds. The use of 3DGS enables superior detail and continuous object surfaces, surpassing Text2Room in clarity. Additionally, our Stage 1 panoramic optimization captures more spatial details, and our designed rendering trajectory generates more comprehensive scenes than LucidDreamer. For instance, LucidDreamer’s point clouds are incomplete with visible voids, while Text2Room struggles with clarity, particularly in floor details. In contrast, SceneDreamer360 delivers consistent and aesthetically pleasing indoor scenes that accurately reflect the prompt, demonstrate the superiority of our approach.

Results Comparison

To objectively evaluate the generation quality, we utilized metrics such as CLIP-Score, CLIP-IQA, PSNR, SSIM, and LPIPS. Table 1 presents the quantitative evaluation results. For generated image quality, SceneDreamer360 outperformed LucidDreamer in terms of CLIP-Score, CLIP-IQA-sharp, CLIP-IQA-colorful, and CLIP-IQA-resolution, achieving better scores compared to LucidDreamer’s scores. Due to the significant variations in perspective and incomplete scenes generated by Text2Room, we did not measure its image quality. However, as illustrated in Fig. 4, the consistency of the scenes generated by Text2Room is notably poor, often resulting in unrealistic scenarios. These results demonstrate the significant advantage of our method in generating high-quality and consistent 3D multiview images. For render quality of the 360-degree scenes, we evaluated the generated images by calculating the average of metrics. Our method outperformed others in terms of PSNR, SSIM, and LPIPS, demonstrating the effectiveness of our approach.

Ablation Study

We conducted ablation experiments on two critical modules: panoramic image enhancement and point cloud fusion, to investigate the effectiveness of our method. The key ablation configurations included: “Standard”, “W/o enhance”, “W/o alignment”, and “W/o enhance & alignment”. As shown in

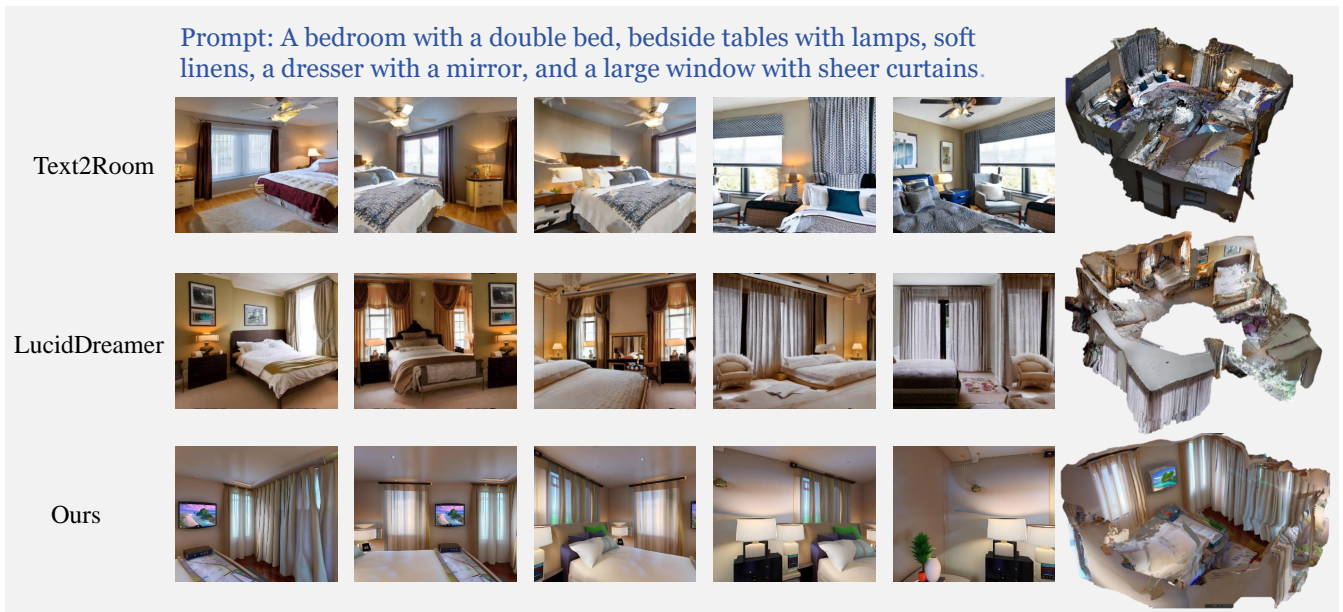


Figure 4: The visualization comparison of the proposed SceneDreamer360 between current methods. The images on the left show the new viewpoint renderings, while the images on the right display the spatial views of the generated 3D scenes.

Method	Image Quality				Render Quality		
	CLIP-Score \uparrow	Sharp \uparrow	Colorful \uparrow	Resolution \uparrow	PSNR \uparrow	SSIM \uparrow	LPIPS \downarrow
Text2Room(Höller et al. 2023)	-	-	-	-	19.29	0.728	0.206
LucidDreamer(Chung et al. 2023)	0.2110	0.9437	0.3230	0.4757	29.56	0.922	0.039
SceneDreamer360	0.2534	0.9877	0.3602	0.7082	35.74	0.963	0.035

Table 1: Comparison of image and render quality across different methods.



Figure 5: The ablation study of SceneDreamer360.

Fig. 5, removing the enhancement module resulted in a loss of finer details, while omitting the alignment module led to noticeable visual discontinuities. The reconstruction without both modules produced worst results, losing both detail and spatial consistency. Additionally, we measured the quantitative performance of the reconstructed images across different configurations, as presented in Table 2. This indicates that removing the alignment module causes a more significant decline in metrics than removing the enhancement module, highlighting the alignment module’s crucial role in maintaining consistent spatial generation.

Method	PSNR \uparrow	SSIM \uparrow	LPIPS \downarrow
Standard	34.96	0.962	0.037
W/o enhance	30.36	0.947	0.011
W/o alignment	10.30	0.365	0.732
W/o enhance & alignment	9.70	0.281	0.803

Table 2: Quantitative comparison of different settings.

Conclusion

In this study, we introduce a novel text-driven method, SceneDreamer360, which generates 3D panoramic scenes by leveraging large diffusion models, enabling the creation of high-quality scenes without constraints to specific target domains. First, we generate highly coherent panoramic images from input text, producing multi-view consistent, high-quality images that are seamlessly integrated into 3D space as point clouds. Next, we apply 3D Gaussian splatting to further enhance the quality of the 3D scenes. By optimizing panoramic image generation and processing, combined with 3D Gaussian splatting, SceneDreamer360 excels in generating complex 3D scenes with fine-grained details and high resolution. Extensive experiments demonstrate that SceneDreamer360 consistently produces high-quality, diverse 3D

scenes under various conditions. Overall, SceneDreamer360 provides an efficient, high-quality solution for text-to-3D scene conversion, contributing to future advancements in 3D scene generation.

References

- Achlioptas, P.; Diamanti, O.; Mitliagkas, I.; and Guibas, L. 2018. Learning representations and generative models for 3d point clouds. In *International conference on machine learning*, 40–49. PMLR.
- Bar-Tal, O.; Yariv, L.; Lipman, Y.; and Dekel, T. 2023. Multidiffusion: Fusing diffusion paths for controlled image generation.
- Bhat, S. F.; Birkl, R.; Wofk, D.; Wonka, P.; and Müller, M. 2023. Zoedepth: Zero-shot transfer by combining relative and metric depth. *arXiv preprint arXiv:2302.12288*.
- Chan, E. R.; Monteiro, M.; Kellnhofer, P.; Wu, J.; and Wetzstein, G. 2021. pi-GAN: Periodic Implicit Generative Adversarial Networks for 3D-Aware Image Synthesis. *arXiv:2012.00926*.
- Chung, J.; Lee, S.; Nam, H.; Lee, J.; and Lee, K. M. 2023. Luciddreamer: Domain-free generation of 3d gaussian splatting scenes. *arXiv preprint arXiv:2311.13384*.
- Cohen-Bar, D.; Richardson, E.; Metzger, G.; Giryes, R.; and Cohen-Or, D. 2023. Set-the-scene: Global-local training for generating controllable nerf scenes. In *Proceedings of the IEEE/CVF International Conference on Computer Vision*, 2920–2929.
- Fridman, R.; Abecasis, A.; Kasten, Y.; and Dekel, T. 2024. Scenescape: Text-driven consistent scene generation. *Advances in Neural Information Processing Systems*, 36.
- Goodfellow, I. J.; Pouget-Abadie, J.; Mirza, M.; Xu, B.; Warde-Farley, D.; Ozair, S.; Courville, A.; and Bengio, Y. 2014. Generative Adversarial Networks. *arXiv:1406.2661*.
- Hessel, J.; Holtzman, A.; Forbes, M.; Bras, R. L.; and Choi, Y. 2021. Clipscore: A reference-free evaluation metric for image captioning. *arXiv preprint arXiv:2104.08718*.
- Ho, J.; Jain, A.; and Abbeel, P. 2020. Denoising diffusion probabilistic models. *Advances in neural information processing systems*, 33: 6840–6851.
- Höllerin, L.; Cao, A.; Owens, A.; Johnson, J.; and Nießner, M. 2023. Text2room: Extracting textured 3d meshes from 2d text-to-image models. In *Proceedings of the IEEE/CVF International Conference on Computer Vision*, 7909–7920.
- Hu, E. J.; Shen, Y.; Wallis, P.; Allen-Zhu, Z.; Li, Y.; Wang, S.; Wang, L.; and Chen, W. 2021. Lora: Low-rank adaptation of large language models. *arXiv preprint arXiv:2106.09685*.
- Jain, A.; Mildenhall, B.; Barron, J. T.; Abbeel, P.; and Poole, B. 2022. Zero-shot text-guided object generation with dream fields. In *Proceedings of the IEEE/CVF conference on computer vision and pattern recognition*, 867–876.
- Kerbl, B.; Kopanas, G.; Leimkühler, T.; and Drettakis, G. 2023. 3D Gaussian Splatting for Real-Time Radiance Field Rendering. *ACM Trans. Graph.*, 42(4): 139–1.
- Lei, J.; Tang, J.; and Jia, K. 2023. Rgb2: Generative scene synthesis via incremental view inpainting using rgb2 diffusion models. In *Proceedings of the IEEE/CVF Conference on Computer Vision and Pattern Recognition*, 8422–8434.
- Li, J.; and Bansal, M. 2024. Panogen: Text-conditioned panoramic environment generation for vision-and-language navigation. *Advances in Neural Information Processing Systems*, 36.
- Li, P.; Tang, C.; Huang, Q.; and Li, Z. 2024. Art3d: 3d gaussian splatting for text-guided artistic scenes generation. *arXiv preprint arXiv:2405.10508*.
- Ma, Y.; Zhan, D.; and Jin, Z. 2024. FastScene: Text-Driven Fast 3D Indoor Scene Generation via Panoramic Gaussian Splatting. *arXiv preprint arXiv:2405.05768*.
- Mildenhall, B.; Srinivasan, P. P.; Tancik, M.; Barron, J. T.; Ramamoorthi, R.; and Ng, R. 2021. Nerf: Representing scenes as neural radiance fields for view synthesis. *Communications of the ACM*, 65(1): 99–106.
- Murtagh, F. 1991. Multilayer perceptrons for classification and regression. *Neurocomputing*, 2(5-6): 183–197.
- Nguyen-Phuoc, T.; Li, C.; Theis, L.; Richardt, C.; and Yang, Y.-L. 2019. Hologan: Unsupervised learning of 3d representations from natural images. In *Proceedings of the IEEE/CVF International Conference on Computer Vision*, 7588–7597.
- Nguyen-Phuoc, T. H.; Richardt, C.; Mai, L.; Yang, Y.; and Mitra, N. 2020. Blockgan: Learning 3d object-aware scene representations from unlabelled images. *Advances in neural information processing systems*, 33: 6767–6778.
- Niemeyer, M.; and Geiger, A. 2021. GIRAFFE: Representing Scenes as Compositional Generative Neural Feature Fields. *arXiv:2011.12100*.
- Poole, B.; Jain, A.; Barron, J. T.; and Mildenhall, B. 2022a. Dreamfusion: Text-to-3d using 2d diffusion. *arXiv preprint arXiv:2209.14988*.
- Poole, B.; Jain, A.; Barron, J. T.; and Mildenhall, B. 2022b. Dreamfusion: Text-to-3d using 2d diffusion. *arXiv preprint arXiv:2209.14988*.
- Qian, G.; Mai, J.; Hamdi, A.; Ren, J.; Siarohin, A.; Li, B.; Lee, H.-Y.; Skorokhodov, I.; Wonka, P.; Tulyakov, S.; et al. 2023. Magic123: One image to high-quality 3d object generation using both 2d and 3d diffusion priors. *arXiv preprint arXiv:2306.17843*.
- Radford, A.; Kim, J. W.; Hallacy, C.; Ramesh, A.; Goh, G.; Agarwal, S.; Sastry, G.; Askell, A.; Mishkin, P.; Clark, J.; et al. 2021. Learning transferable visual models from natural language supervision. In *International conference on machine learning*, 8748–8763. PMLR.
- Ramakrishnan, S. K.; Gokaslan, A.; Wijmans, E.; Maksymets, O.; Clegg, A.; Turner, J.; Undersander, E.; Galuba, W.; Westbury, A.; Chang, A. X.; et al. 2021. Habitat-matterport 3d dataset (hm3d): 1000 large-scale 3d environments for embodied ai. *arXiv preprint arXiv:2109.08238*.

- Ramesh, A.; Pavlov, M.; Goh, G.; Gray, S.; Voss, C.; Radford, A.; Chen, M.; and Sutskever, I. 2021. Zero-shot text-to-image generation. In *International conference on machine learning*, 8821–8831. Pmlr.
- Rombach, R.; Blattmann, A.; Lorenz, D.; Esser, P.; and Ommer, B. 2022. High-resolution image synthesis with latent diffusion models. In *Proceedings of the IEEE/CVF conference on computer vision and pattern recognition*, 10684–10695.
- Shu, D. W.; Park, S. W.; and Kwon, J. 2019. 3d point cloud generative adversarial network based on tree structured graph convolutions. In *Proceedings of the IEEE/CVF international conference on computer vision*, 3859–3868.
- Song, J.; Meng, C.; and Ermon, S. 2020. Denoising diffusion implicit models. *arXiv preprint arXiv:2010.02502*.
- Takikawa, T.; Litalien, J.; Yin, K.; Kreis, K.; Loop, C.; Nowrouzezahrai, D.; Jacobson, A.; McGuire, M.; and Fidler, S. 2021. Neural geometric level of detail: Real-time rendering with implicit 3d shapes. In *Proceedings of the IEEE/CVF Conference on Computer Vision and Pattern Recognition*, 11358–11367.
- Tang, S.; Zhang, F.; Chen, J.; Wang, P.; and Furukawa, Y. 2023. MVDiffusion: Enabling Holistic Multi-view Image Generation with Correspondence-Aware Diffusion. *arXiv*.
- Tulsiani, S.; Su, H.; Guibas, L. J.; Efros, A. A.; and Malik, J. 2017. Learning shape abstractions by assembling volumetric primitives. In *Proceedings of the IEEE Conference on Computer Vision and Pattern Recognition*, 2635–2643.
- Vahdat, A.; Williams, F.; Gojcic, Z.; Litany, O.; Fidler, S.; Kreis, K.; et al. 2022. Lion: Latent point diffusion models for 3d shape generation. *Advances in Neural Information Processing Systems*, 35: 10021–10039.
- Wang, C.; Chai, M.; He, M.; Chen, D.; and Liao, J. 2022. Clip-nerf: Text-and-image driven manipulation of neural radiance fields. In *Proceedings of the IEEE/CVF Conference on Computer Vision and Pattern Recognition*, 3835–3844.
- Wang, H.; Xiang, X.; Fan, Y.; and Xue, J.-H. 2024. Customizing 360-degree panoramas through text-to-image diffusion models. In *Proceedings of the IEEE/CVF Winter Conference on Applications of Computer Vision*, 4933–4943.
- Wang, J.; Chan, K. C.; and Loy, C. C. 2023. Exploring clip for assessing the look and feel of images. In *Proceedings of the AAAI Conference on Artificial Intelligence*, volume 37, 2555–2563.
- Wang, X.; Xie, L.; Dong, C.; and Shan, Y. 2021. Real-rgan: Training real-world blind super-resolution with pure synthetic data. In *Proceedings of the IEEE/CVF international conference on computer vision*, 1905–1914.
- Yavartanoo, M.; Chung, J.; Neshatavar, R.; and Lee, K. M. 2021. 3dias: 3d shape reconstruction with implicit algebraic surfaces. In *Proceedings of the IEEE/CVF International Conference on Computer Vision*, 12446–12455.
- Zhang, C.; Wu, Q.; Cruz Gambardella, C.; Huang, X.; Phung, D.; Ouyang, W.; and Cai, J. 2024. Taming Stable Diffusion for Text to 360° Panorama Image Generation. In *Proceedings of the IEEE/CVF Conference on Computer Vision and Pattern Recognition*.
- Zhang, L.; Rao, A.; and Agrawala, M. 2023. Adding conditional control to text-to-image diffusion models. In *Proceedings of the IEEE/CVF International Conference on Computer Vision*, 3836–3847.
- Zhou, H.; Cheng, X.; Yu, W.; Tian, Y.; and Yuan, L. 2024a. HoloDreamer: Holistic 3D Panoramic World Generation from Text Descriptions. *arXiv preprint arXiv:2407.15187*.
- Zhou, L.; Du, Y.; and Wu, J. 2021. 3d shape generation and completion through point-voxel diffusion. In *Proceedings of the IEEE/CVF international conference on computer vision*, 5826–5835.
- Zhou, S.; Fan, Z.; Xu, D.; Chang, H.; Chari, P.; Bhargava, T.; You, S.; Wang, Z.; and Kadambi, A. 2024b. DreamScene360: Unconstrained Text-to-3D Scene Generation with Panoramic Gaussian Splatting. *arXiv preprint arXiv:2404.06903*.